Journal of the European Ceramic Society **14** (1994) 529–537

Uniaxial Tensile and Creep Behaviour of an Alumina Fibre-Reinforced Ceramic Matrix Composite: I. Experimental Study

F. Lamouroux, M. Steen & J. L. Vallés

Institute for Advanced Materials, Joint Research Centre, European Commission, PO Box 2, 1755 ZG Petten, The Netherlands

(Received 18 April 1994; accepted 8 June 1994)

Abstract

The uniaxial tensile and creep behaviour of an alumina fibre-reinforced silicon carbide composite is studied. The damage mechanisms during tensile loading are identified on the basis of the elastic response and in-situ *morphological analysis. Tensile tests show that the composite presents a pseudo-ductile behaviour due to matrix microcracking and fibre–matrix debonding. Temperature induces changes in the tensile behaviour because of variations in load transfer conditions and in the axial residual stress borne by the fibres and the matrix. The creep curves at 1100°C under vacuum present an extended tertiary part, especially at low creep stress. The unloading–reloading loops periodically performed during creep show a progressive decrease in longitudinal stiffness. Progressive interface debonding during creep is invoked to explain: (i) the strain rate increase during tertiary creep, (ii) the decrease of the elastic modulus and (iii) the large fibre pull-out observed on the creep fracture surface. The different creep rupture modes at low and high stresses are related to the capability of the remaining intact fibres to support the overload failure of the first fibres.*

Die Eigenschaften von aluminiumoxidfaserverstärktem Siliziumcarbid im einachsigen Zug- und Kriechversuch werden untersucht. Die Schädigungsmechanismen unter Zugbelastung werden an Hand der Änderungen des elastischen Verhaltens und in-situ *Gefügeuntersuchungen identifiziert. Die Ergebnisse der Zugversuche zeigen, daß dieser Verbundwerkstoff ein pseudoduktiles Verhalten aufweist, welches auf die Bildung von Matrixmikrorissen und der Ablösung der Fasern von der Matrix zurückgeführt werden kann. Temperaturänderungen bewirken Veränderungen in der Kraftübertragung zwischen und in den Restspannungen in der Matrix und den Fasern und haben daher einen direkten Einfluß auf das Zugverhalten des Werkstoffs. Die Kriechkurven des bei 1100°C unter Vakuum getesteten Materials weisen einen ausgeprägten tertiären Bereich auf, besonders bei geringen Spannungen. Das periodische Ent- und Belasten der Probe während des Kriechversuchs verursacht einen kontinuierlichen Abfall des E-Moduls. Das andauernde Ablösen der Fasern von der Matrix wird für folgende Beobachtungen verantwortlich gemacht: (i) die Zunahme der Dehnung während des tertiären Kriechens, (ii) das Absinken des E-Moduls, (iii) das Vorhandensein von vielen, weit herausgezogenen Fasern in der Bruchfläche. Die unterschiedlichen Kriechbruchmechanismen bei niedriger und hohen mechanischen Belastungen stehen in direkter Verbindung mit der Fähigkeit der intaktbleibenden Fasern, die erhöhte mechanische Spannung nach dem Bruch der ersten Fasern zu übernehmen.*

Le comportement en traction et en fluage uniaxial d'un composite constitué de fibres d'alumine et d'une matrice en carbure de silicium est étudié. Les mécanismes d'endommagement du matériau durant le chargement en traction sont identifiés sur les bases de la réponse élastique et de l'analyse morphologique in-situ. *Les essais de traction montrent que le composite présente un comportement mécanique du type pseudo-ductile lié au développement de fissures matricielles et de décohésions fibre-matrice. La température induit des modifications du comportement en traction en raison de la variation des conditions de transfert de charge ainsi que des contraintes thermiques résiduelles axiales supportées par les fibres et la matrice. Les courbes de fluage à 1100°C sous vide présentent un important domaine tertiaire, particulièrement à basse contrainte de fluage. Les boucles de déchargement-rechargement effectuées périodiquement pendant les essais de fluage montrent une décroissance progressive du module d'élasticité longitudinal. Une décohésion progressive de l'interface durant le fluage est proposée pour*

Journal of the European Ceramic Society 0955-2219/94/$7.00

expliquer: (i) l'accroissement de la vitesse de deformation durant le regime tertiaire, (ii) la décroissance du module d'élasticité et (iii) l'important déchaussement des fibres observé sur les surfaces de rupture par fluage. Les différences de modes de rupture par fluage à basse et à haute contraintes sont corrélées à la capacité des fibres non rompues à supporter la surcharge provoquée par la rupture des premières fibres.

1 Introduction

Many applications of advanced materials require high-temperature strength in aggressive environments. Ceramic materials present attractive properties such as thermal stability, oxidation and corrosion resistance, and a low density. They suffer, however, from the serious drawback of high flaw sensitivity and low toughness. Ceramic fibre-reinforced ceramic matrix composites (CMCs) have been developed to overcome the lack of toughness and thereby increase the reliability of ceramic materials. Also, the favourable thermomechanical properties of CMCs make them potential candidates for high-temperature structural applications. Many studies performed on CMCs have highlighted the important role played by damage mechanisms in controlling the mechanical behaviour.[1-6] In particular, matrix microcracking and interfacial debonding contribute to a non-linear/non-brittle mechanical behaviour and thereby result in remarkable improvements in toughness. Damage mechanisms are also expected to play a role in sustained loading applications involving creep, where they are related to the mismatch in creep properties between fibre and matrix.

To summarise the creep behaviour of CMCs, Holmes & Chermant[7] proposed a classification in terms of the creep mismatch ratio (CMR), defined as the ratio of the intrinsic creep rate of the fibre to that of the matrix. For composites with CMR <1, typically the SiC(Nicalon)/CAS (calcium aluminium silicate) materials, the main damage mechanism occurring during creep is periodic fibre fracture. On the other hand, for materials with CMR > 1, such as SiC(SCS-6)/ RBSN (reaction bonded silicon nitride) composites, matrix microcracking is the dominant mode of damage. The damage mechan-isms strongly influence the creep kinetics and consequently the creep life of CMCs. For example, in the case of the uniaxial tensile creep of SiC(SCS-6)/HPSN (hot pressed silicon nitride) at 1200°C in air and under 250 MPa, Holmes *et al.*[8] have observed that the behaviour of the composite is governed by the loading rate, dependent on the presence or absence of initial matrix microcracking. The uniaxial tensile creep under vacuum of an Al_2O_3(f)/SiC composite has recently been studied for applied stresses above the first matrix cracking stresses.[9,10] It was shown that the creep behaviour exhibits primary and tertiary stages, the extent of each stage depending on the level of the applied stress. In this way, at 1100°C, creep tests perfomed at low stresses (σ < 150 MPa) lead to a more extended tertiary part and a higher failure strain (over 5%) as compared to tests performed at high stress levels (σ > 150 MPa), where the failure strain is around 2%. In terms of the minimum creep rate, the analysis of the results suggests a double stress dependence with stress exponents of 9·5 and 4·5 at low and high stresses, respectively. At high stresses, the composite creep behaviour can be entirely explained on the basis of the creep of non-incorporated fibres, whereas such fibre-dominated creep is masked by unsaturated matrix cracking in the low stress range.

In this study, attention is focussed on the damage phenomena occurring during uniaxial tensile and creep loading of the same Al_2O_3(f)/SiC composite. Both the elastic response in tests with unload–reload cycles and morphological analyses are used to characterise the damage mechanisms. Modelling of the tertiary creep behaviour of this CMC on the basis of these damage mechanisms is presented in a companion article.[11]

2 Experimental Procedure

2.1 Material

The composite studied consists of woven alumina fibres (Sumitomo) incorporated in a silicon carbide matrix. The fibres making up the 2D plain weave structure contain 85% by weight of γ-alumina and 15% of amorphous silica. The maximum temperature of the fibre manufacturing process is 970° (final heat treatment), which causes alumina to crystallise with a small grain size of around 12 nm. The γ-phase remains stable up to 1127°C, a transformation into mullite occurring at higher temperatures.[12]

In a first step, the fibres are coated with a carbon layer (interphase) in order to promote the desired pseudo-ductile behaviour of the composite. The thickness of this carbon layer ranges from 0·5 to 1 μm. The silicon carbide matrix is subsequently formed *in situ* by isothermal chemical vapour infiltration (CVI). The as-processed composite presents a fibre volume fraction of 0·4 and approximately 20% in volume of porosity. The main properties of the composite constituents are summarised in Table 1.

Table 1. Some characteristics of the Al_2O_3/SiC composite constituents[9–15]

Properties	*Al_2O_3 fibres*	*SiC matrix*
Type	Sumitomo	ICVI/CVD
Density (g cm^{-3})	3·25	3·2
Young's modulus at RT (GPa)	160	420
Young's modulus at 1100°C (GPa)	140	420
Elastic strain to rupture at RT (%)	0·6	0·05
CTE ($\times 10^{-6}$ K^{-1})	8·8	4·5
Creep rate at 1100°C, 100 MPa (s^{-1})	$1{\cdot}5 \times 10^{-8}$	4×10^{-11}
Creep rate at 1100°C, 500 MPa (s^{-1})	8×10^{-7}	—
Stress exponent	2·2–4·4	1
Weibull modulus at RT	3·7	—
Weibull modulus at 1100°C	6–8	—
Volume fraction	0·4	0·4

The Sumitomo fibres are composed of γ-alumina and amorphous silica.
ICVI/CVD = isothermal chemical vapour infiltration/chemical vapour deposition from a CH_3SiCl_3 gaseous precursor.

2.2 Mechanical tests

Uniaxial tensile and creep tests were performed in a machine equipped with an induction heater and a graphite susceptor. Flat rectangular cross-section specimens of 10×3 (mm^2) with a total length of 200 mm were tested under vacuum ($P_t < 10^{-5}$ mbar) in order to avoid oxidative attack of the interphases after the formation of matrix cracks. In the room-temperature (RT) tests, strain was recorded by a clip-on extensometer, while a contacting extensometer equipped with silicon carbide rods was used at high temperature. For all tests, the strain and stress data were recorded digitally and stored for further evaluation. Other details of the experimental set-up are given in Ref. 9. Isothermal tensile tests, some featuring unloading–reloading cycles, were performed up to failure at room temperature and at 1100°C. Creep tests were carried out at 1100°C and at stresses of 100 and 170 MPa. The tests were periodically interrupted by an unloading–reloading cycle in order to observe the changes in the elastic response of the composite. The unloading and reloading rate was around 2 MPa s^{-1} in both the tensile and the creep tests. Since in the creep tests symmetrical hysteresis loops are obtained, it can be assumed that this rate is high enough to limit the recovery phenomena during the cycle.

2.3 Morphological analysis

Morphological observations were performed before and after mechanical testing by optical microscopy. An optical setup was developed to allow *in-situ* observation of the damage process during room-temperature tensile loading. Good optical resolution was obtained by mirror polishing one of the thickness faces of the specimen. The microscope, with a 50 to 250 times magnification range, was installed in front of the polished face and connected to a photo/video camera.

3 Results

3.1 Morphological investigations of the as-received material

A low magnification optical micrograph of a polished section of the as-received composite shows the 2D woven texture of the alumina fibres (single arrows in Fig. 1(a)) and the silicon carbide matrix (white area). Porosity is apparent both inside and between the fibre tows (double arrows in Fig. 1(a)). The presence of microcracks in the matrix inside the fibre tows (single arrows in Fig. 1(b)) indicates that some damage is already produced during processing. At higher magnification, it is also possible to observe partial debonding between fibre and matrix (double arrows in Fig. 1(b)). The plane of the matrix microcracks is oriented perpendicular to the local fibre axis. It is worth noting that these microcracks extend through the thin matrix mantles surrounding individual fibres located inside a fibre tow, and that they are bridged by the fibres. Moreover, it is observed that these cracks arrest inside the thick matrix deposited around the fibre tows (triple arrows).

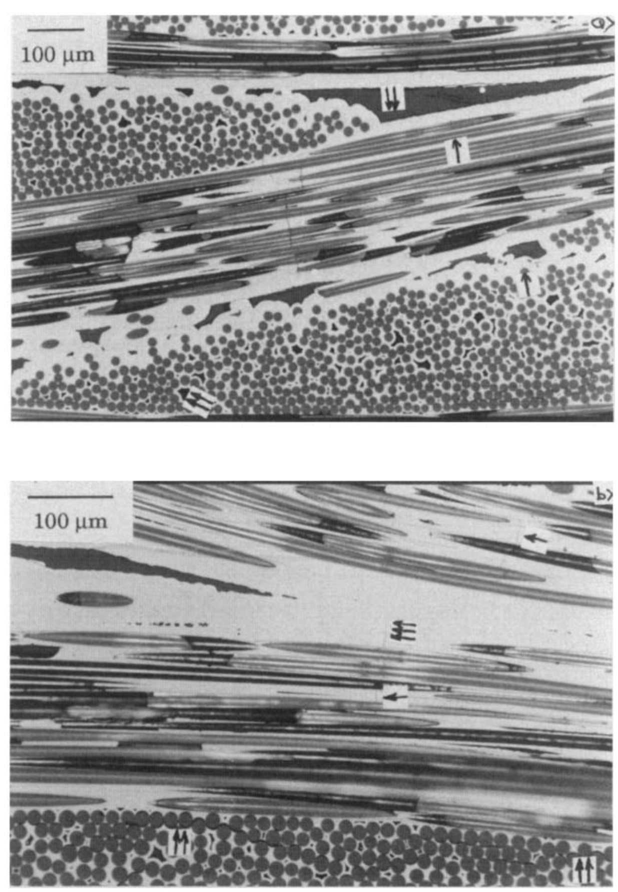

Fig. 1. Cross-section micrograph of a 2D Al_2O_3/SiC composite in the as-received state: (a) matrix appears in white, fibres and porosity are respectively indicated by single and double arrows; (b) matrix microcracking and fibre–matrix partial debonding are observed in the as-processed material.

3.2 Tensile tests

3.2.1 Room temperature tensile behaviour

Three distinct regions can be observed in the tensile curves obtained at room temperature (Fig. 2):

$0 < \sigma < 100$ MPa: Elastic behaviour is observed, characterised by a longitudinal elastic modulus of around 100 GPa. The appearance of the first damage resulting from mechanical loading is usually associated with a decrease in the longitudinal elastic modulus. However, since in the early stages of the damage process the strain related to this decrease is too low to be detected by the extensometer, damage could already be present during part of this linear region.

$100 < \sigma < 130$ MPa: A deviation from linearity is observed in the tensile curve. A small decrease in the elastic modulus is also obtained from the unloading– reloading cycles. Optical analysis of the specimen under load shows the presence of matrix cracks both inside and in between the fibre tows. The crack spacing is of the same order as that observed in the as-received composite, which corresponds to only the matrix cracks located inside fibre tows.

$\sigma > 130$ MPa: A significant decrease in stiffness is obtained, accompanied by an increase in the width of the loops. Optical analysis of the specimen under load shows an increase in microcrack opening up to around 10 μm, but seemingly only a very limited multiplication of the matrix microcracking takes place, because the crack spacing observed on the external surface does not change significantly. At stresses close to 180 MPa optical microscopy shows the failure of some fibres. Moreover, matrix cracks parallel to the load axis start developing, especially between the fibre tows. Near the composite rupture stress ($\sigma \approx 180$ MPa), the coupled longitudinal and transverse strains cause additional multi-cracking of the matrix and further fibre failure. Composite failure is accompanied by gross delamination and sliding between the layers.

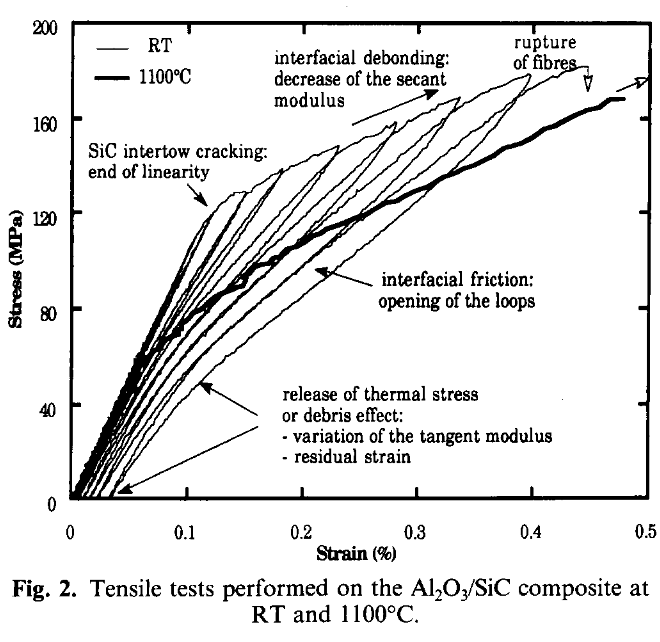

Fig. 2. Tensile tests performed on the Al_2O_3/SiC composite at RT and 1100°C.

A close observation of the tensile curve with unloading–reloading cycles shows that each cycle presents two distinct regions upon unloading, characterised by a decrease and an increase in the value of the longitudinal stiffness. The region of increasing stiffness may be related to: (i) the relaxation of the residual stresses induced by processing, upon the development of matrix cracking and interfacial debonding and/or (ii) the blocking of the microcracks closure by silicon carbide fragments. Furthermore, it can be noticed that the transition stress between the two regions decreases as damage accumulates.

Figure 3 shows that the longitudinal stiffness of the composite decreases monotonically with increasing accumulated tensile strain. Its value is calculated as the average secant modulus of the high stress region of the loop, which corresponds to the regime of free opening of the matrix cracks. This decrease in modulus continues up to failure, which indicates that a saturation of the damage mechanisms is not attained during tensile loading at room temperature.

3.2.2 High-temperature tensile behaviour

The tensile test performed at 1100°C shows qualitatively similar behaviour as the one at room temperature, as can be seen in Fig. 2. However, the end of the linear part at 1100°C occurs for a smaller strain of 0·06 %, compared to 0·12 % at room temperature. Moreover, the decrease in the longitudinal elastic modulus with tensile strain is less pronounced at high temperature (see Fig.3).

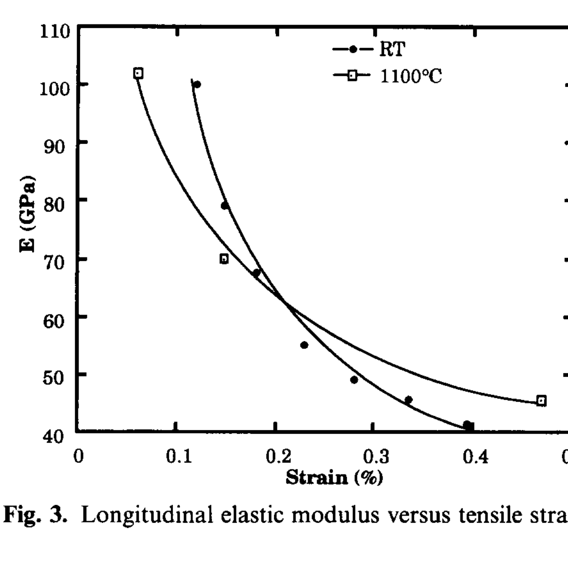

Fig. 3. Longitudinal elastic modulus versus tensile strain.

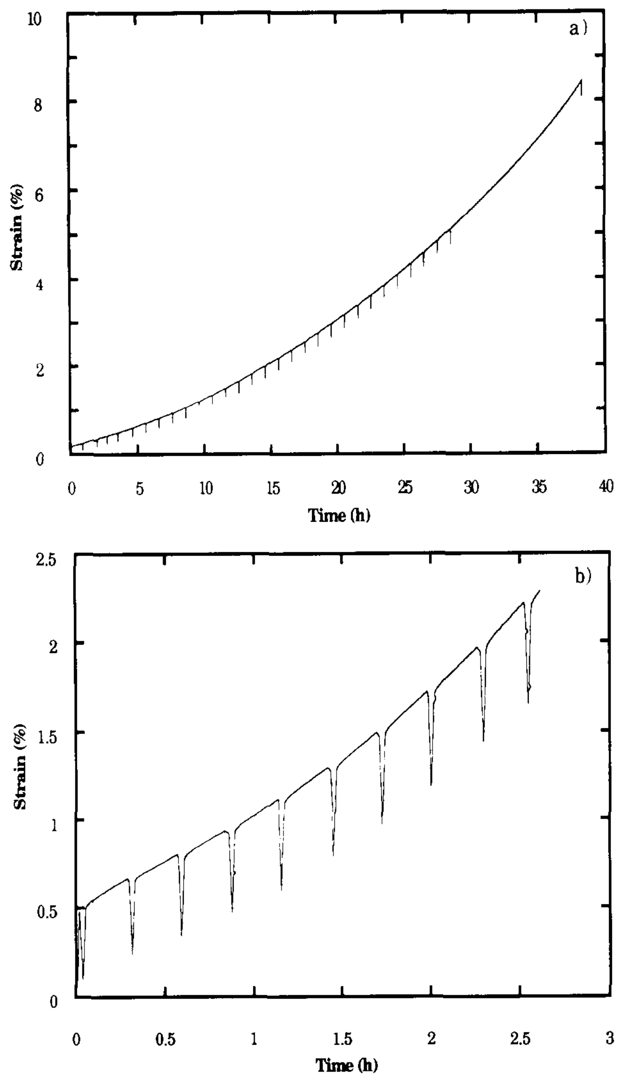

Fig. 4. Creep curves in tests incorporating unloading–reloading cycles performed on a 2D Al_2O_3/SiC composite at 1100°C under (a) 100 MPa and (b) 170 MPa.

3.3 High-temperature creep tests

As can be seen in Table 1, the Al_2O_3/SiC composite studied here exhibits a fibre creep rate higher than that of the matrix (i.e. CMR > 1). Since the creep behaviour of CMCs is expected to be strongly influenced by the damage state of the composite, uniaxial creep tests in the tensile mode were performed at 1100°C under vacuum for stresses of 100 and 170 MPa. As for the tensile tests, unloading–reloading cycles were included. For the creep stress of 170 MPa, cycles were recorded until rupture, while they were recorded only during 75% of the 100 MPa creep test. However, for the latter test, the elastic modulus was also recorded just before composite failure.

The creep curves, which are shown in Fig. 4, present an extended tertiary stage, especially at low stresses, which is characterised by a monotonical increase in the strain rate with time. The strain to rupture reaches 8·5% at 100 MPa, whereas it is a smaller 2·5% at 170 MPa. An additional creep test has been performed at 100 MPa without unloading–reloading cycles. Since the resulting creep curve does not differ from that obtained when including the cycles, it can be assumed that these do not significantly affect the creep behaviour. The creep fracture surfaces exhibit abundant fibre pull-out, with lengths of several millimetres (see Fig. 5). The matrix presents a microcrack network characterised by large cracks of several hundreds of microns in width, oriented perpendicular to the load axis and bridged by fibres (white lines in Fig. 5). Figure 6 shows a bimodal crack spacing distribution, which clearly reflects the existence of both intertow and intratow matrix cracking, after a 100 MPa creep test.

The strain rate of the composite has been plotted in Fig. 7. For the two levels of stress, the strong decrease in the primary stage is followed by a tertiary stage where the strain rate increases linearly with time. The secondary stage is reduced to a single point. At this inflection point, the minimum strain rate is 2×10^{-7} s^{-1} and $1{\cdot}5 \times 10^{-6}$ s^{-1} at 100 MPa and 170 MPa, respectively. In the last stage of the 100 MPa test, the creep strain strongly

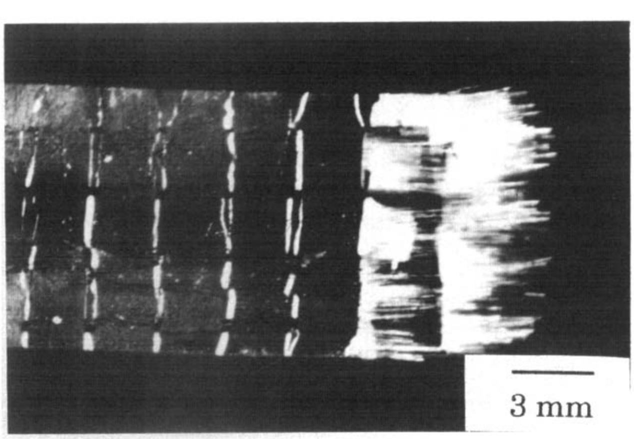

Fig. 5. Optical micrograph of the fracture surface of the composite after creep at 1100°C under 100 MPa showing the fibre pull-out and the large opened microcracks perpendicular to the load axis.

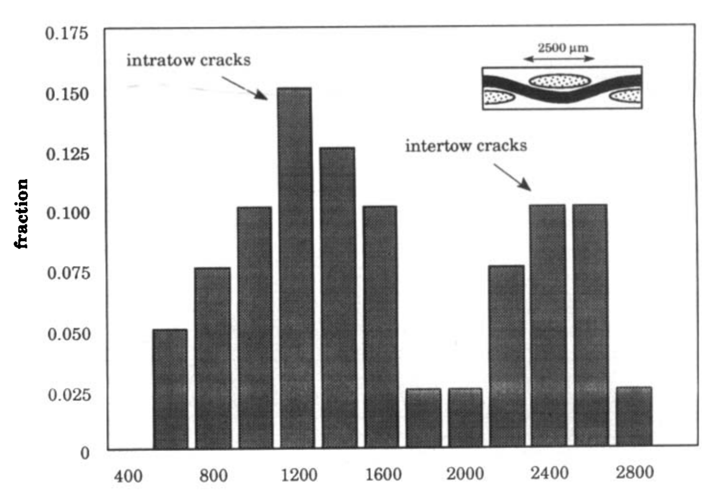

Fig. 6. Distribution of the crack spacing for a 2D Al_2O_3/SiC composite after creep failure at 1100°C under 100 MPa.

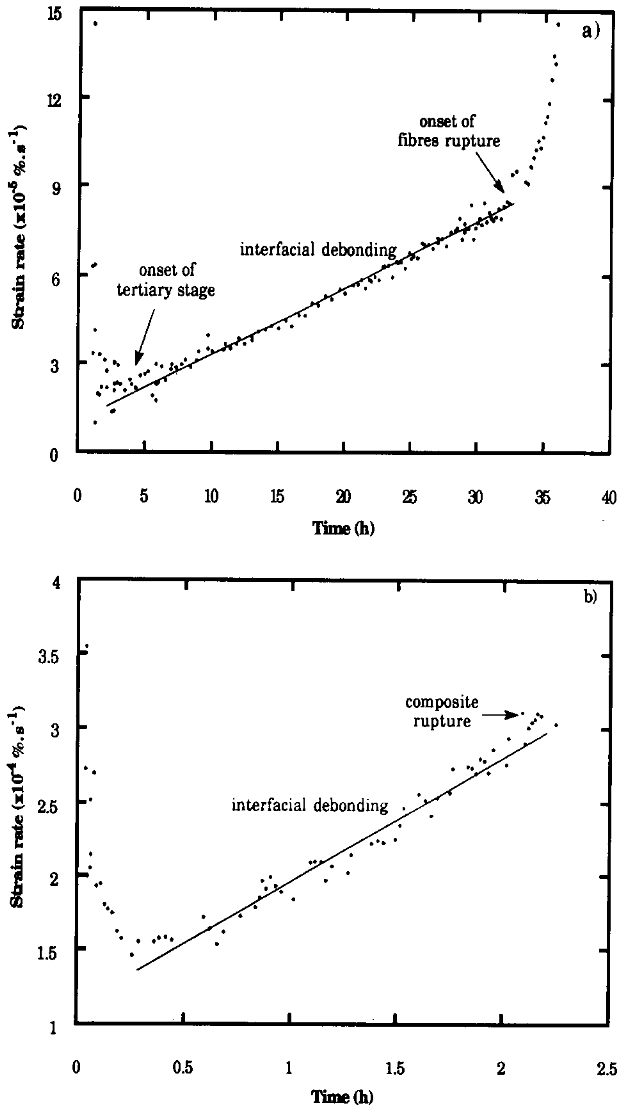

Fig. 7. Evolution of the strain rate during creep tests at 1100°C under (a) 100 MPa and (b) 170 MPa.

accelerates, while at 170 MPa the linear increase with time continues up to rupture.

As for the tensile tests, the evolution of the longitudinal elastic modulus with creep strain has been determined from the unloading–reloading

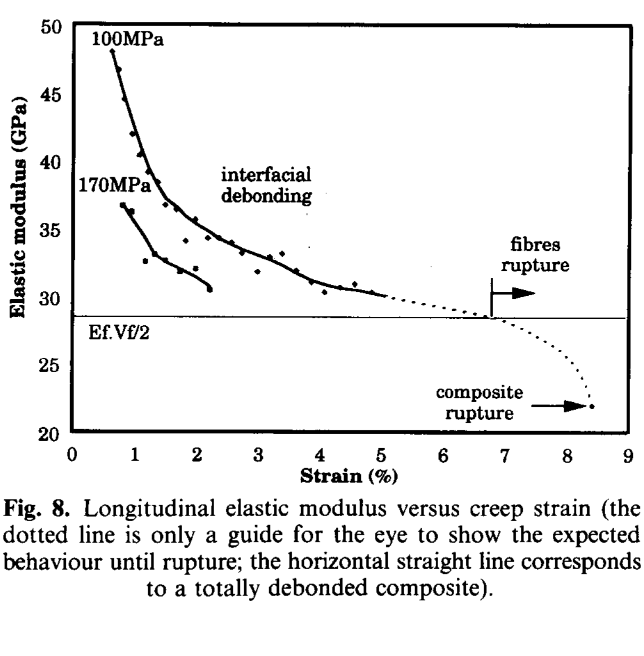

Fig. 8. Longitudinal elastic modulus versus creep strain (the dotted line is only a guide for the eye to show the expected behaviour until rupture; the horizontal straight line corresponds to a totally debonded composite).

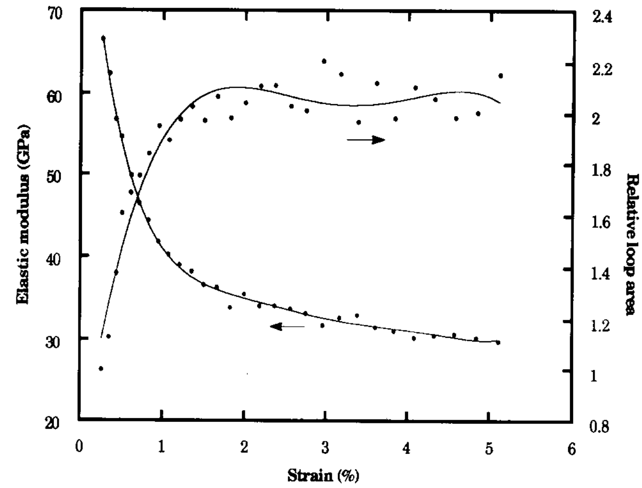

Fig. 9. Elastic modulus and relative loop area versus creep strain at 1100°C under 100 MPa.

cycles performed during the creep tests. Creep is accompanied by a decrease of the elastic modulus, which tends to a value of around 30 GPa at low creep stress (Fig. 8). Moreover, the relative area of the unloading–reloading loops, calculated as the ratio of the area of a loop to the area of the first one, only increases at the beginning of the creep test and then stays at a constant value during the remaining part of the test (Fig. 9).

4 Discussion

4.1 Manufacturing related damage

Optical microscopy investigations have shown that the as-received material exhibits matrix microcracks and interfacial debonding. Matrix microcracks seem to initiate inside the fibre tows and arrest in the matrix surrounding the fibre tow. Since the alumina fibres have a coefficient of thermal expansion (CTE) higher than that of silicon carbide (see Table 1), thermal stresses develop when the composite cools down from the CVI manufacturing temperature. As a consequence of this thermal expansion mismatch, at room temperature the fibre is expected to be under axial tension and the matrix under axial compression. However, the presence of matrix cracks inside the tows in the as-received condition suggests the existence of residual *tensile* stresses in the intratow matrix. This can be explained as follows. At the interface between an individual fibre and its surrounding thin matrix shell inside a given tow, a geometric constraint prevents the axial residual stresses from changing sign abruptly. Instead, in the radial direction, the tensile residual stress profile gradually decreases as it extends into the thin intratow matrix, which is then expected to fail in the presence of a critical defect. The thick matrix surrounding the fibre tows, however, is subjected to residual compressive stresses, which prevent the cracks from propagating. Consequently, the cracks generated inside the fibre tows stop at the periphery of the fibre tow, as observed in Fig. 1. After cooling from the manufacturing temperature the interface is expected to be under radial tension. This stress state is responsible for the interfacial debonding.

4.2 Tensile behaviour

When a tensile load is applied to the composite, a linear elastic behaviour is observed until the arrested intratow microcracks start to propagate through the intertow matrix. The value of the initial longitudinal elastic modulus is smaller than that expected from the rule of mixtures ($E_0 \approx$ 100 GPa, instead of around 200 GPa). This is due to the presence of intratow matrix cracks and interfacial debonding.

The composite presents a tough behaviour because of the presence of damage in the matrix and at the interface. *In-situ* morphological analysis during loading has shown that matrix microcracking is limited to a small part of the stress–strain curve after the elastic region. At higher stress levels ($\sigma >$ 130 MPa), the dominating damage mechanisms are interfacial debonding and fibre sliding. They result in a residual strain after unloading and in the hysteresis loops to open up with increasing stress.

The damage mechanisms (matrix cracking, interface debonding and fibre sliding) are influenced by the stress state in the constituents of the composite and the load transfer condition between fibre and matrix. The load transfer depends on: (i) chemical bonds between the fibre and the interphase and between the interphase and the matrix, and (ii) mechanical bonds due to interfacial roughness and thermal clamping stresses caused by the CTE mismatch between fibre and matrix. In the case of this Al_2O_3(f)/SiC composite, increasing temperature induces a decrease of the axial compressive stress in the intertow matrix. This agrees with the fact that the deviation from a linear behaviour occurs at a lower strain at 1100°C than at room temperature (Fig. 2). An increase in temperature also causes a larger radial expansion of the fibre than of the matrix. This results in an improved load transfer between fibre and matrix, which is reflected in Fig. 2 by a higher tangent modulus after the elastic part, and in Fig. 3 by a slower decrease of the elastic modulus at the higher temperature.

4.3 Creep behaviour

In the experiments performed, loading to the applied creep stress causes the intratow matrix cracks present in the as-received condition to propagate into the intertow regions. Subsequently, a stress redistribution between the fibres and the matrix takes place because of the mismatch in their creep properties. Since the creep rate of the alumina fibre exceeds that of the matrix (see Table 1), the faster creeping (i.e. weaker) fibres shed their load to the slower creeping (i.e. stronger) matrix. This stress redistribution gives rise to a primary creep stage for the composite, characterised by a decreasing creep rate. In view of the fact that the number of intertow matrix cracks does not differ significantly from the number of intratow cracks, and that an increase in the matrix stress does not cause additional matrix cracking, it can safely be assumed that additional damage does not occur during the primary creep stage. Thus, at the end of primary creep the damage state is characterised by a microcracked matrix and locally debonded fibres. As in the tensile tests, complete fibre–matrix debonding is not attained after the stress redistribution stage in the creep tests. Consequently, there exists a potential for extra damage accumulation during further creep.

Since CMR > 1, and the fibres are partially debonded from the matrix, and thus subjected to the full applied creep stress over a certain length, the creep behaviour of the composite is expected to be dominated by the creep of the debonded fraction of the fibres. The creep behaviour of the Sumitomo fibre has been studied by Lesniewski *et al.*,[12] who have reported on primary and secondary creep of the fibres in the temperature range 800–1150°C, both in air and in argon. At 1100°C and 0·5 GPa, the stationary creep rate is affected by the environment, having values of 8×10^{-7} s^{-1} and 6×10^{-6} s^{-1} in air and in argon respectively. The stress exponent at the same temperature is 2·2 in air and 4·4 in argon. It is worth noting that, unlike the composite, the alumina fibre presents a secondary creep stage. Thus, in order to explain the absence of composite stationary creep, an analysis which is based exclusively on the creep of the constituents is not sufficient. In what follows, an approach based on the potential for damage accumulation is explored.

The macroscopic manifestation of damage in terms of a decreasing elastic modulus after primary creep of the composite can be explained by progressive fibre–matrix debonding and/or fibre failure, since additional microcracking of the matrix does not occur after the applied creep stress has been reached. The rate of decrease in the elastic modulus slows down during creep and the modulus tends to 30 GPa, especially at creep stress of 100 MPa, a value which corresponds to that of a composite where the load is entirely taken up by the fibres

($E_f V_f/2 \approx 28$ GPa). Also, large fibre pull-out lengths are observed on the fracture surfaces after creep and the matrix cracks with large crack opening have the same average spacing as that observed in tensile tests. All these observations point to the direction of fibre–matrix debonding, rather than fibre rupture, being the dominant damage mechanism.

Fibre–matrix debonding always results from chemical or mechanical changes at the interface. Under sustained high-temperature loading, reactions between the carbon interphase and the alumina fibres can lead to a degradation of the interfacial strength properties. However, extensive fibre surface degradation on the fracture surface of the composite after creep at 1100°C has not been observed.[9] A more plausible explanation for interfacial debonding during creep is offered by the important creep strain accumulation in the fibre, giving rise to radial fibre shrinkage. Radial fibre contraction necessarily induces changes in the interfacial stress state, which can lead to progressive fibre–matrix debonding. As a consequence, the fraction of fibre directly exposed to the maximum stress increases, and this causes the strain rate of the composite to increase. This results in a tertiary creep stage of the composite, which is in fact related to the stationary creep of the alumina fibres combined with progressive interfacial debonding.

Fibre–matrix debonding involves a decrease of the composite elastic modulus, which is usually accompanied by an increase in the work of friction. Such an increase manifests itself by an increasing opening of the unloading–reloading loops, as has been observed under tensile loading at room temperature (Fig. 2). In the creep tests, however, the increase in the debonding length is associated with a radial shrinkage of the fibres. The increase of friction surface between fibre and matrix is thus compensated by a decrease of the Coulomb frictional shear stress through a decrease of the radial clamping stress caused by the radial contraction, giving rise to a constant hysteretic area (Fig. 9).

During the tertiary stage, the creep rate shows initially a linear increase with time (Fig. 7). At the end of this linear part, composite rupture occurs for the high applied stress whereas at low stress the creep rate shows a sudden increase. This can be explained by the fibre failure process: at low stress, fibre failure induces a stress redistribution among the remaining fibres, which does not necessarily imply composite rupture. Instead, there is an increase of the stress on the remaining fibres, and consequently of the composite creep rate (see Fig. 7(a), for time >30h). In this way, successive fibre failure leads to a progressive increase of the creep rate until composite rupture, giving rise to an extended tail to the creep curve. In contrast, at high stresses the overload produced by the failure of the first fibres induces an avalanche of fibre failures, resulting in a catastrophic rupture of the composite (see Fig. 7(b)).

5 Conclusions

The tensile and creep behaviour of a 2D Al_2O_3/SiC composite under uniaxial loading has been studied. Morphological analyses gave an insight about the different damage processes occurring during room-temperature tensile loading. Both tensile and creep tests incorporating unloading–reloading cycles provided the longitudinal elastic response as a function of accumulated strain. From this investigation, several conclusions can be drawn:

(1) In the as-received condition, i.e. after cooling down from the manufacturing temperature, the composite already exhibits damage in the form of matrix microcracking inside the fibre tows and interface debonding.
(2) Tensile tests performed at room and high temperatures show that the decrease in the longitudinal elastic modulus is only associated with an interfacial debonding mechanism, since additional matrix cracking and fibre failure do not occur.
(3) The creep curves at 1100°C exhibit primary and tertiary stages, the secondary stage being reduced to an inflection point. The tertiary stage is quite extended, especially at low stress. Unloading from and reloading to the applied creep stress shows that during the tertiary stage the longitudinal elastic modulus progressively decreases.
(4) Progressive fibre–matrix debonding explains: (i) the decrease of the longitudinal elastic modulus in the tensile and creep tests, (ii) the increase of the strain rate during tertiary creep and (iii) the large fibre pull-out observed on the creep fracture surfaces.
(5) The creep failure mode is stress dependent. Namely, at low stress successive fibre failure induces a strong increase in the composite creep rate, whereas at high stress it leads to a catastrophic composite failure.

Acknowledgements

This work has been performed within the Research and Development Programme of the European Commission. The authors thank P. Young for his assistance in mechanical testing and A. Baritello and

R. De Cat for their help with the *in-situ* optical investigations. The authors acknowledge Société Européenne de Propulsion for providing the composite material.

References

1. Quenisset, J. M., Mécanismes d'endommagement des matériaux composites. In *23e Colloque du Groupe Français de Rhéologie*, Cermub Editor, Bordeaux, 1988, pp. 1–41.
2. Evans, A. G. & Marshall, D. B., In *Mat. Res. Soc. Symp. Proc. 120*, ed. F. D. Lemkey, S. G. Fishman, A. G. Evans & J. R. Strife, 1988, pp. 213–46.
3. Talreja, R., A continuum mechanics characterization of damage in composite materials. *Proc. R. Soc. Lond.*, **A399** (1987) 196–216.
4. Rouby, D. & Reynaud, P., Fatigue behaviour related to interface modification during load cycling in ceramic–matrix fibre composites. *Composites Science and Technology*, **48** (1993) 109–18.
5. Evans, A. G. & Marshall, D. B., Failure mechanics in ceramic fibre–ceramic matrix composites. *J. Am. Ceram. Soc.*, **68**(5) (1985) 225–31.
6. Charalambides, P. G. & Evans, A. G., Debonding properties of residually stressed brittle-matrix composites. *J. Am. Ceram. Soc.*, **72**(5) (1989) 746–53.
7. Holmes, J. W. & Chermant, J. L., Creep behaviour of fibre-reinforced ceramic matrix composites. In *High Temperature Ceramic Matrix Composite, Proceedings of the 6th European Conference on Composite Materials*, ed. R. Naslain, J. Lamon & D. Doumeingts, Bordeaux, 1993, pp. 633–47.
8. Holmes, J. W., Park, Y. H. & Jones, W. J., Tensile creep and creep-recovery behavior of a SiC-fiber–Si_3N_4-matrix composite. *J. Am. Ceram. Soc.*, **76**(5) (1993) 1281–93.
9. Adami, J. N., Comportement en fluage uniaxial sous vide d'un composite 2D Al_2O_3/SiC. Thèse de l'Ecole Polytechnique de Zürich, Switzerland, 1992.
10. Steen, M. & Vallés, J. L., Uniaxial creep of ceramic matrix composites: experiments and modelling. In *Mechanisms and Mechanics of Composite Fracture*, ed. R. B. Bhagat, S. G. Fishman & R. J. Arsenault. ASM, Pittsburgh, 1993.
11. Lamouroux, F., Vallés, J. L. & Steen, M., Uniaxial tensile and creep behaviour of an alumina fibre–reinforced ceramic matrix composite: II. Modelling of tertiary creep. *J. Eur. Ceram. Soc.*, **14** (1994) 539–48.
12. Lesniewski, Ch., Aubin, C. & Bunsell, A. R., Property–structure characterization of a continuous fine alumina–silica fibre. *Composites Science and Technoloy*, **37** (1990) 63–78.
13. Naslain, R., *Introduction aux Matériaux Composites*. CNRS-IMC, Vol. 2, Bordeaux, 1985.
14. Courtright, E. L., Engineering property limitation of structural ceramics and ceramic composites above 1600°C. *Ceram. Eng. Sci. Proc.*, **12**(9–10) (1991) 1725–44.
15. Cannon, W. R., Creep of Ceramics—I. Mechanical characteristics. *J. Mater. Sci.*, **12** (1977) 1–50.